Structure of an Allosteric Inhibitor of LFA-1 Bound to the I-Domain Studied by Crystallography, NMR, and Calorimetry[†,‡]

Matthew P. Crump,*[,§] Thomas A. Ceska,[||] Leo Spyracopoulos,[⊥] Alistair Henry,[||] Sarah C. Archibald,[||] Rikki Alexander,[||] Richard J. Taylor,[||] Stuart C. Findlow,[§] James O'Connell,[||] Martyn K. Robinson,[||] and Anthony Shock[||]

School of Biological Sciences, University of Southampton, Bassett Crescent East, Southampton SO16 7PX, U.K., Celltech R&D, 216 Bath Road, Slough, Berks SL1 4EN, U.K., and MRC Group in Protein Structure and Function, Department of Biochemistry, University of Alberta, Edmonton, Alberta T6G 2H7, Canada

Received August 8, 2003; Revised Manuscript Received December 18, 2003

ABSTRACT: LFA-1 (lymphocyte function-associated antigen-1) plays a role in intercellular adhesion and lymphocyte trafficking and activation and is an attractive anti-inflammatory drug target. The α-subunit of LFA-1, in common with several other integrins, has an N-terminally inserted domain (I-domain) of ∼200 amino acids that plays a central role in regulating ligand binding to LFA-1. An additional region, termed the I-domain allosteric site (IDAS), has been identified exclusively within the LFA-1 I-domain and shown to regulate the function of this protein. The IDAS is occupied by small molecule LFA-1 inhibitors when cocrystallized or analyzed by $^{15}N-^{1}H$ HSQC (heteronuclear single-quantum coherence) NMR (nuclear magnetic resonance) titration experiments. We report here a novel arylthio inhibitor that binds the I-domain with a K_d of 18.3 nM as determined by isothermal titration calorimetry (ITC). This value is in close agreement with the IC_{50} (10.9 nM) derived from a biochemical competition assay (DELFIA) that measures the level of inhibition of binding of whole LFA-1 to its ligand, ICAM-1. Having established the strong affinity of the arylthio inhibitor for the isolated I-domain, we have used a range of techniques to further characterize the binding, including ITC, NMR, and X-ray crystallography. We have first developed an effective ITC binding assay for use with low-solubility inhibitors that avoids the need for ELISA-based assays. In addition, we utilized a fast NMR-based assay for the generation of I-domain−inhibitor models. This is based around the collection of HCCH-TOCSY spectra of LFA-1 in the bound form and the identification of a subset of side chain methyl groups that give chemical shift changes upon binding of LFA-1 inhibitors. This subset was used in two-dimensional $^{13}C-^{15}N$ and ^{15}N-filtered and -edited two-dimensional NMR experiments to identify a minimal set of intraligand and ligand−protein NOEs, respectively (nuclear Overhauser enhancements). Models from the NMR data were assessed by comparison to an X-ray crystallographic structure of the complex, confirming that the method correctly predicted the essential features of the bound ligand.

LFA-1[1] is a member of the integrin family of glycoproteins, molecules known to be expressed on a wide range of cell types and capable of mediating cell−cell and cell−matrix interactions (for reviews, see refs *1*−*3*). The integrins are heterodimeric in structure, with LFA-1 being composed of α-subunits (αL) and β-subunits (β2). The ligands for LFA-1 are members of the intercellular adhesion molecule (ICAM) family such as ICAM-1, ICAM-2, and ICAM-3. LFA-1 is of considerable interest because there is evidence from both animal studies (*4*, *5*) and clinical data in human psoriasis (*6*) indicating that it plays a key role in regulating T-cell trafficking and activation.

The structural basis for integrin activation is not completely understood, but the recently determined crystal structure of the αVβ3 integrin (*7*, *8*) has provided some important clues. The N-termini of all integrin α subunits contain seven homologous segments of ∼60 amino acids each, which come together to form what has been called a seven-bladed β-propeller. Ligand binding occurs at an interface between the β-propeller on the α-chain and a region on the β-subunit usually termed the A-domain.

[†] This work was supported by an equipment grant (055640) from the Wellcome Trust to the University of Southampton (M.P.C. and S.C.F.).

[‡] The coordinates for the X-ray and NMR structures of LFA-1 with a bound ligand have been deposited in the Brookhaven Protein Data Bank as entry 1RD4.

* To whom correspondence should be addressed. Present address: School of Chemistry, University of Bristol, Cantock's Close, Bristol BS8 1TS, U.K. Phone: 0117 3317163. Fax: 0117 9298611. E-mail: matt.crump@bristol.ac.uk.

[§] University of Southampton.

[||] Celltech R&D.

[⊥] University of Alberta.

[1] Abbreviations: (125−311,C125A,W189R), I-domain double mutant used in the NMR studies; HSQC, heteronuclear single-quantum coherence; ICAM, intercellular adhesion molecules; IDAS, I-domain allosteric site; ITC, isothermal titration calorimetry; LFA-1, lymphocyte function-associated antigen-1; MIDAS, metal ion-dependent adhesion site; NMR, nuclear magnetic resonance; NOESY, nuclear Overhauser effect spectroscopy; SAR-by-NMR, structure−activity relationships by nuclear magnetic resonance; TOCSY, total correlation spectroscopy; TROSY, transverse relaxation optimized spectroscopy.

10.1021/bi035422a CCC: $27.50
Published on Web 02/13/2004

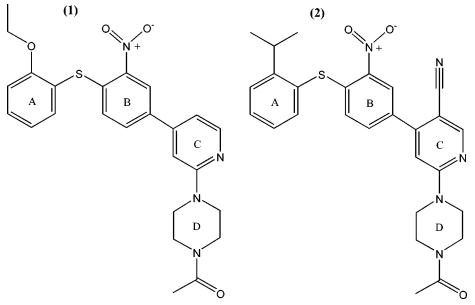

FIGURE 1: Structures of inhibitor compounds **1** and **2**.

LFA-1, in common with approximately half of the integrins, contains a region of ~200 amino acids termed the I-domain. This is attached to the amino terminus of the αL β-propeller and is known to play a direct role in ligand binding (*9*−*13*). Analyses of other I-domain-containing α-chains such as αM, α1, and α2 support these findings and, in particular, have identified five oxygenated residues containing the conserved DxSxS sequence on the "upper" face of the I-domain that constitutes a divalent cation binding region (or MIDAS) (*14*). Indeed, a similar motif has been identified in the β-chain A-domain which is important for ligand binding activity in integrins which lack an I-domain (*8*, *14*). For LFA-1, ligand binding is associated with coordination of Mg^{2+} mediated by residues within both the MIDAS of αL and by an acidic residue donated by the ligand (*15*−*18*). X-ray crystallographic analyses of LFA-1 in complex with ICAM-1 have now very accurately pinpointed the coordination of Glu31 of the ICAM-1 domain with the I-domain Mg^{2+} and a dramatic conformational rearrangement of I-domain Glu241 to form a new salt bridge with Lys39 of ICAM-1 (*19*).

Structural analysis of various I-domains indicates that there are two possible conformations: an "open" form that represents the ligand binding conformation and a "closed" conformation that is not competent to bind ligand (*14*, *20*, *21*). In fact, it has been possible to introduce mutations in both αM and αL that lock open and closed conformations with predicted effects on functional ligand binding when incorporated into the heterodimeric integrin (*22*−*27*). Most crystal and NMR structures for the αL I-domain represent closed conformations (*20*, *28*, *29*), although one NMR study (*30*) did demonstrate specific changes in residues in the MIDAS region of αL upon ligand binding. Importantly, this last study also identified a second region, located between the C-terminal α-helix and the β-sheet of the I-domain, that is affected upon ligand binding and which they termed the I-domain allosteric site (IDAS). The functional relevance of the IDAS has been strengthened by data with several low-molecular weight antagonists of LFA-1 that have all been shown to bind in this region (*28*, *31*, *32*). The first class of these compounds was based on a *p*-arylthio cinnamide framework containing the arylthio group (A-ring) and a properly substituted cinnamyl moiety (B-ring) [Figure 1 (**1**)]. The second class of compounds was based around the novel hydantoin framework, while more recently, a third series of novel 1,4-diazepane-2-ones have been shown to bind and inhibit LFA-1 (*33*). The I-domain in combination with these inhibitors crystallizes in the closed conformation, suggesting that the compounds bind to and/or favor the formation of this form. Mutations in the LFA-1 I-domain that lock it in the open form also render the integrin resistant to inhibition by antagonists (*25*). Two-dimensional (2D) ^{15}N heteronuclear single-quantum correlation ($^{15}N-^{1}H$ TROSY-HSQC) spectra of the uniformly ^{15}N-labeled LFA-1 I-domain were recorded in several of these studies, allowing the location and orientation of binding of the inhibitor at the IDAS to be unequivocally determined (*34*); in addition, the "SAR-by-NMR" (*35*) approach has been very successful for screening small molecules as potential inhibitors of LFA-1.

This paper describes the NMR and X-ray crystallographic characterization of a new antagonist [Figure 1 (**1**)] that incorporates an additional ring (C) in place of the double bond of the cinnamide group. The ring was designed to improve hydrophobic interactions with the IDAS binding pocket, maintain extra rigidity, and aid in projecting the cyclic amide (D) away from the binding pocket (*36*). We have analyzed the binding of compound **1** to LFA-1 with ITC and determined that it binds the LFA-1 I-domain with an IC_{50} of 18.3 nM, one of the lowest reported in the literature. We have used an NMR screen to generate models of the **1**−LFA-1 I-domain complex that confirm that the inhibitor has the desired binding conformation. In both cases, a small set of NOEs between **1** and the I-domain was sufficient to position the inhibitor at the IDAS and, coupled with the intramolecular NOEs, reveal the conformation of the aromatic ring system in the protein-bound form. This analysis could be completed rapidly and was generally applicable to other inhibitors, including **2**.

MATERIALS AND METHODS

Protein Production. The recombinant LFA-1 I-domain used in these studies corresponds to residues Cys125−Gly311 of the αL chain of LFA-1. The I-domain fragment was cloned by PCR from human lymphocyte cDNA and expressed in the plasmid vector pPROEX Htb (GIBCO/BRL). Two mutations were introduced into the structure for the NMR studies; Cys125 was changed to Ala to improve the stability of the expressed product, and Trp189 was changed to Arg to make the protein comparable with that used in the published crystal structure (*20*) [herein termed (125−311,C125A,W189R)]. The recombinant protein produced for crystallography contained only the W189R mutation. An N-terminal six-His tag was introduced followed by a TEV protease motif. This results in the mature protein having a five-amino acid (GAMGS) N-terminal extension.

The recombinant I-domain was expressed in *Escherichia coli* XL-1B cells. For unlabeled protein, LB medium was used. For isotopically ^{15}N-labeled or ^{15}N- and ^{13}C-labeled protein, Celtone-N or Celtone-CN (Spectra Stable Isotopes, Columbia, MD) was used, respectively. Expression levels were typically in excess of 350 mg per liter of bacterial culture. Recombinant material was in the form of inclusion bodies.

Protein purification was carried out as follows. Cell pellets were extracted according to a method adapted from Bohmann and Tjian (*37*). All volumes were based on 4 L of original culture volume, and all steps were performed at 4 °C. Cell pellets were resuspended in 72 mL of buffer A [10 mM Tris-HCl, 100 mM KCl, 2 mM DTT, 2 mM PMSF, and 25% (w:v) sucrose (pH 8.5)]. After the addition of 18 mL of buffer B [300 mM Tris-HCl, 100 mM EDTA, and 4 mg/mL hen

egg lysozyme (pH 8.5)], the solution was incubated on ice for 30 min with occasional swirling. Following incubation, 90 mL of buffer C [1 M LiCl, 20 mM EDTA, and 0.5% (v:v) NP-40] was added and the solution passed through a French press (Aminco, Urbana, IL) at 20 000 psi. The material was centrifuged at 16000*g* for 15 min at 4 °C and the supernatant discarded. The pellet was resuspended in 100 mL of buffer D [10 mM Tris-HCl, 0.5 M LiCl, 0.1 mM EDTA, 1 mM DTT, 1 mM PMSF, and 0.5% (v:v) NP-40 (pH 8.5)], passed through the French press, and centrifuged as described above. This stage with buffer D was repeated and the pellet resuspended in 100 mL of buffer E [10 mM Tris-HCl, 0.1 mM EDTA, 1 mM DTT, 1 mM PMSF, and 0.5% (v:v) NP-40 (pH 8.5)], passed through the French press, and centrifuged as described above. This stage with buffer E was then repeated. Protein pellets were stored at −70 °C.

Protein refolding was carried out as follows. Protein pellets were resolubilized in 6 M GuHCl (3 mL of GuHCl/L of original culture volume). Solubilized protein was clarified by centrifugation at 48000*g* for 30 min at 4 °C. At this stage, the isolated I-domain was >95% pure, was quantified spectrophotometrically (the theoretical molar extinction coefficient at 280 nm is 12 800), and was determined to be at a concentration of greater than 100 mg/mL. The I-domain was diluted to 1 mg/mL in 8 M deionized urea and 50 mM Tris-HCl (pH 8.0) and incubated at 20 °C for 60 min. The solution was diluted rapidly with cold 50 mM Tris-HCl, 1 mM $MgCl_2$, and 5% (v:v) glycerol (pH 8.0) to 50 μg/mL and incubated with stirring at 4 °C for 16 h. A Q-Sepharose Fast Flow column (Amersham Biosciences, Little Chalfont, Bucks, U.K.) was equilibrated with 50 mM Tris-HCl, 5% (v:v) glycerol, and 1 mM $MgCl_2$ (pH 8.0). The refolded I-domain was loaded onto the column, and the column was washed in equilibration buffer and eluted with a 10 column volume gradient into equilibration buffer containing 1 M NaCl. Pooled fractions containing the I-domain were cleaved with TEV protease for 24 h at 20 °C at a TEV:I-domain weight:weight ratio of 1:50. Cleaved material was purified by negative selection on Ni−NTA affinity beads (Qiagen). Purified, cleaved material was concentrated and diafiltered into NMR sample buffer [10 mM sodium phosphate, 150 mM NaCl, 1 mM $MgCl_2$, 0.01% (w:v) NaN_3, and 5% (v:v) D_2O (pH 7.4)] or crystallization buffer [10 mM Tris-HCl, 5% (v:v) glycerol, and 5 mM 2-mercaptoethanol (pH 7.5)]. Protein integrity was confirmed by N-terminal sequencing, electrospray mass spectrometry, SDS−PAGE, and analytical gel filtration. Typical final yields were 20−30% expressed recombinant protein.

Isothermal Titration Calorimetry. Isothermal titration calorimetry was performed using a VP-ITC system (MicroCal, Inc., Northampton, MA). Since compound **1** is not water soluble at high concentrations, the standard experimental procedure was reversed so that **1** was placed in the cell and the I-domain placed in the syringe.

The I-domain was concentrated to 221.7 μM in a buffer containing 20 mM Tris base (pH 7.5), 150 mM NaCl, and 1 mM $MgCl_2$ using an Amicon stirred cell fitted with a YM10 membrane. Compound **1** was added directly to the ultrafiltrate in neat DMSO to give a final concentration of 19.6 μM in a 2% DMSO solution. The same concentration of DMSO was added to the I-domain to equalize the solvent concentration in the syringe and the cell.

After being degassed, the solution of **1** was placed in the cell (1.4 mL) and the I-domain in the syringe. The latter was titrated into the cell at 180 s intervals in a total of 55 injections of 5 μL at 30 °C. Data were analyzed and fitted using the data analysis software supplied by MicroCal (Origin version 5.0).

Monitoring of Complex Formation by NMR Spectroscopy. (125−311,C125A,W189R) of LFA-1 was isotopically labeled with ^{13}C and ^{15}N nuclei using the purification and refolding outlined above. NMR samples contained 1.5 mM uniformly ^{15}N- and ^{13}C-labeled LFA-1 I-domain in 10 mM sodium phosphate buffer (pH 7.4), 150 mM NaCl, 1 mM $MgCl_2$, 0.01% (w:v) NaN_3, and 5% (v:v) D_2O. All data sets were recorded at 22 °C. Binding of **1** to the I-domain was monitored by acquiring 2 h $^{15}N-^{1}H$ TROSY-HSQC experiments (*38*) in the presence and absence of **1**. Titration of compound **1** was considered complete when those peaks that exhibited chemical shift changes showed just a single peak at the new chemical shift position and when a slight turbidity was observed in the solution. This was removed by centrifugation prior to subsequent analysis. A similar approach was applied to the analysis of compound **2**.

NMR Structure Calculations of the Compound 1−I-Domain Complex. NMR experiments were performed on a Varian *INOVA* spectrometer (Varian Associates, Palo Alto, CA) equipped with a 14.1 T (^{1}H 600 MHz) magnet and a triple-resonance *Z*-gradient probe. Backbone and side chain assignments of (125−311,C125A,W189R) were obtained from HNCA, CBCACONNH, HNCACB, and HCCH-TOCSY experiments combined with comparison to chemical shifts reported previously for the native I-domain (*29*). Following formation of a complex with **1**, HNCA and HCCH-TOCSY spectra were reacquired and new assignments made. The HNCA spectrum was assigned largely for the sake of completeness as the amide assignments are not explicitly used in the structural analysis described below. The assignments of the complexed nonisotopically enriched inhibitor were made using 2D ^{13}C and ^{15}N double-filtered NOESY and TOCSY experiments. NOEs between the I-domain and **1** were obtained from a 2D ^{15}N-filtered NOESY spectrum. To check the general applicability of this approach, an identical analysis was pursued for compound **2**.

Nine intermolecular inhibitor **1**−protein NOEs and 10 inhibitor **1** intramolecular (inter-ring) NOEs were assigned from the 2D spectra and incorporated as soft-well potentials in an X-PLOR version 3.81 simulated annealing protocol (*39*). A starting model consisting of the X-ray structure of the I-domain and inhibitor **1** manually docked near the IDAS (20 Å from the diaryl bridge to the approximate center of the IDAS) was generated. Ten models were then calculated using 50 ps of high-temperature molecular dynamics followed by 30 ps of cooling and finally 1000 steps of Powell minimization. Topology and parameter files for inhibitor **1** were generated using XPLO-2D (*40*). All backbone and side chain atoms of the I-domain were fixed outside of a 5 Å radius of inhibitor **1**.

Crystallization. The protein was stored at 28 mg/mL in 10 mM Tris-HCl (pH 7.5), 5 mM βME, and 5% glycerol. For crystallization, the protein was diluted to a final concentration of 0.9 mM in a buffer composed of 6.5 mM Tris-HCl (pH 7.5), 3.25 mM βME, 3.25% glycerol, 100 mM $MgCl_2$, and 1 mM inhibitor, and this was allowed to incubate

Table 1: Data Collection and Refinement Statistics

data collection statistics[a]	
temperature (K)	100
no. of crystals	1
wavelength (Å)	1.5418
resolution range (Å)	40.0−2.4
space group	*P*1
unit cell dimensions	$a = 45.96$ Å, $b = 64.41$ Å, $c = 66.21$ Å, $\alpha = 74.21°$, $\beta = 90.00°$, $\gamma = 87.26°$
no. of measurements used	160725
no. of unique reflections	26155
completeness (%)	91.6 (82.1)
average $I/\sigma(I)$	8.1
R_{merge} (%)	6.8 (22.2)
refined model	
protein residues	A128−A311, B128−B311, C128−C311, D128−D311
no. of water molecules	0
no. of inhibitor molecules	4
geometry	
rmsd for bonds (Å)	0.008
rmsd for angles (deg)	1.18
refinement of model	
R-factor	0.236
R_{free} (10% used)	0.290
average *B*-factor (Å^2)	
protein	14.0
inhibitor molecules	25.6

[a] Data were collected on a MAR research 345 area detector at 100 K and processed with DENZO, and the model was refined with CNX. Data shown in parentheses are for the highest-resolution shell (2.44−2.40 Å).

on ice for 4 h. Equal amounts of the protein solution and a well solution composed of 100 mM sodium acetate (pH 4.6), 200 mM ammonium acetate, and 30% (w:v) PEG4000 were mixed together for hanging drop crystallization. Crystals grew within 4 weeks to a maximal size of 0.10 mm × 0.05 mm × 0.05 mm.

Structure Determination. Crystals were picked up with a cryoloop and briefly passed through the well solution just prior to being flash-frozen in a cryostream. Data were collected on a rotating anode source with a MAR research scanner, reduced with DENZO (*41*), and merged using Scalepack. The molecular replacement solution was determined with MolRep [within CCP4 (*42*)] using the uncomplexed I-domain as the search model [PDB entry 1LFA (*20*)]. Refinement was carried out with CNX (*39*), and the model was manually improved between cycles of refinement using O (*43*). The main chain atoms for all four independent molecules were restrained by noncrystallographic symmetry. The main chain was highly restrained, and the side chains were allowed to move independently because of the different crystal contact environment around each molecule. Individual *B*-factor refinement with restraints was carried out according to a conventional protocol, and in addition, *B*-factors between noncrystallographically related molecules were tightly restrained. The restraint file has been deposited along with the coordinates at the Protein Data Bank. The data collection and refinement statistics are shown in Table 1.

RESULTS AND DISCUSSION

Compound **1** competes with the binding of ICAM-1 to whole LFA-1 in a DELFIA format with an IC_{50} of 10.9 nM (data not shown). Since ICAM-1 does not bind to the isolated

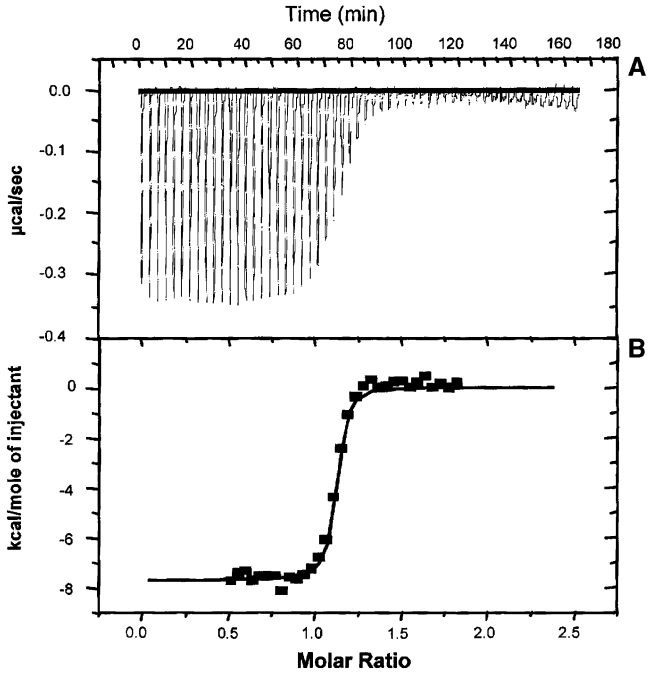

FIGURE 2: Isothermal calorimetry. **(**A) Raw ITC data for the interaction of **1** with the I-domain. The titration consists of 55 additions of 5 μL aliquots of the I-domain (221.7 μM) into the calorimeter cell containing ~1.4 mL of **1** (19.6 μM). (B) Data after peak integration and subtraction of basal values fitted to a simple single-site binding model (solid line).

I-domain, an alternative approach was necessary to demonstrate that **1** binds specifically to this domain. Isothermal titration calorimetry measures the heat changes that occur when two molecules interact. This allows a direct assessment of binding without the need for additional assay components or derivatization. Normally, the small molecule is titrated into a compartment containing the protein, but when solubility is an issue, as in this instance, the binding partners can be reversed.

Representative data are shown in Figure 2. Panel A shows the raw data, and panel B shows the area under the peaks in the top panel, plotted as a function of the ratio of moles of I-domain added to moles of **1**. The calculated best fit based on simple one-site binding was determined after peaks due to heat of dilution had been subtracted. The apparent increase in peak size at the end of the run (panel A) was ignored because this has been observed when protein is used as the titrant into buffer alone (data not shown). The negative displacement of the peaks is typical of an exothermic reaction. The negative value of the enthalpy term ΔH (−7.7 kcal/mol) and the positive value for the entropy term ΔS (10.0 cal mol^{-1} K^{-1}) would suggest that both terms contribute to an overall favorable change in Gibbs free energy (ΔG). The calculated binding stoichiometry (n) of 1.12 is within experimental error for the binding of one molecule of **1** to one molecule of the I-domain. The equilibrium dissociation constant (K_d) was calculated to be 18.3 nM and is comparable with the IC_{50} generated in the ICAM-1−LFA-1 DELFIA assay.

NMR Spectroscopy. Initially, the interaction of **1** with the I-domain was investigated by recording $^{15}N-^{1}H$ TROSY-HSQC spectra of the uniformly labeled I-domain in the absence and presence of **1**. Previous control experiments verified that the presence of ~2−3 μL of DMSO used to

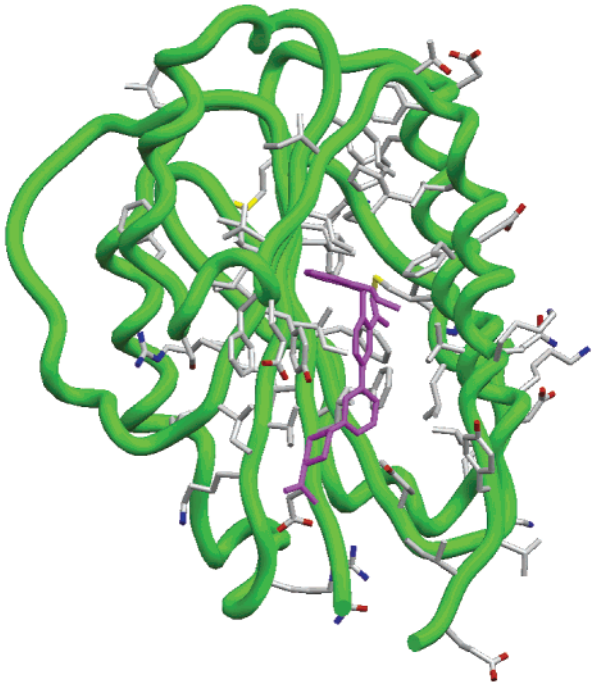

FIGURE 3: Structure of the I-domain highlighting the residues in contact with the inhibitor. The backbone of (125−311,C125A, W189R) is shown as a green ribbon and is taken from the X-ray structure determined in this study. Compound **1** bound to (125−311,C125A,W189R) is shown in purple. The side chains of the residues that shifted in the $^{15}N-^{1}H$ TROSY-HSQC experiment after complete titration (1:1 complex) of **1** are shown, indicating their distribution over the entire molecule.

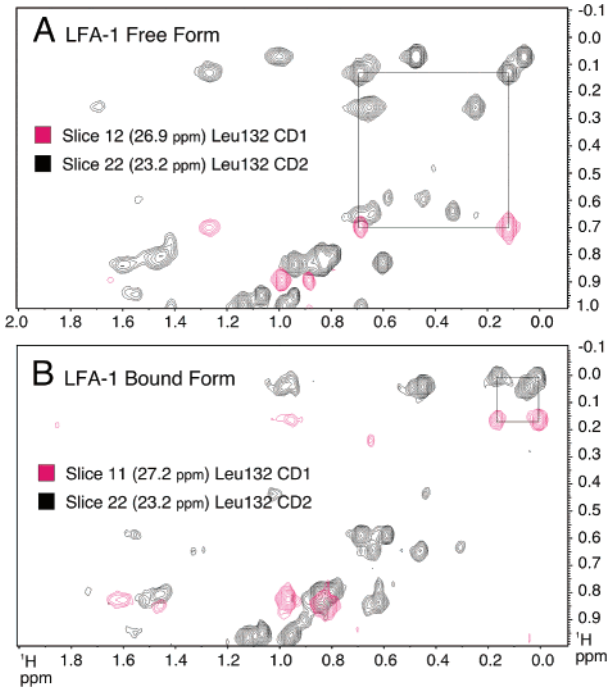

FIGURE 4: ^{13}C slices from the HCCH-TOCSY spectrum of the I-domain in the free form (A) and in complex with **1 (B)**. In panel A, the black and magenta cross-peaks represent the native spectrum of (125−311,C125A,W189R) taken at 26.9 and 23.2 ppm, respectively. The methyl peaks of Leu132 that have these chemical shifts form a symmetric pair indicated by the connecting lines. In panel B, the symmetric pair is indicated at 27.2 and 23.2 ppm. In this case, the Leu132 methyl groups could not be identified from a comparison of proton shifts because of the large pertubation with respect to the free form. However, the uniqueness and similarity of the four ^{13}C shifts allowed its identification.

solubilize **1** prior to addition to the I-domain solution caused no observable perturbation to the chemical shifts observed in the $^{15}N-^{1}H$ TROSY-HSQC data. Numerous chemical shift changes ($\Delta\delta$) are observed upon addition of **1**, and midway through the titration, inspection of the HSQC spectra reveals the appearance of two sets of peaks corresponding to bound and unbound forms of I-domain. This behavior is characteristic of tight binding and is not unexpected given the experimentally determined K_d of 18.3 nM. The chemical shift changes form seven distinct groupings along β-strand 1, helix 1, β-strand 3, β-strand 4, the C-terminus of helix 6, β-strand 5, and helix 7 through to the C-terminus. The changes confirm the binding behavior of **1** mimics that of other I-domain diaryl sulfide inhibitors. However, the binding pocket of the I-domain is only crudely defined by mapping the changes onto the protein structure. Figure 3 shows all of the residues that show shifts in the $^{15}N-^{1}H$ TROSY-HSQC spectrum, and these clearly include numerous shifts from residues that are not close to the IDAS binding site. Such chemical shift changes can be caused by "secondary binding effects" such as changes in the solvation of the protein and most significantly conformational changes that are propagated away from the binding site.

Methyl Scanning. We were interested in applying a faster and noncumbersome NMR method that could rapidly generate structures of protein−inhibitor complexes of this class of molecule. Inhibitors of this class feature multiply substituted aromatic rings, resulting in resonances with well-dispersed downfield chemical shifts and therefore readily interpretable spectra. Upon binding to the I-domain, the aromatic rings can induce sizable chemical shift changes in nearby aliphatic side chain groups of the protein. In particular, methyl groups from Leu, Val, and Ile can be rapidly identified when perturbed from their native chemical shift values in the inhibitor free state. Proton and carbon chemical shifts are both sensitive to short-range ring current effects from aromatic groups, conformational changes in their local covalent structure, and nearby charged groups. The range of methyl chemical shifts in which most carbon resonances appear is from 5 to 30 ppm, which is ~10−20 times larger than the range of proton chemical shifts. However, unlike the protons, they are not directly at the binding interface between the protein and ligand, and therefore when the ligand binds, they give much smaller chemical shift changes than the protons. In general, we observed that the protons give large chemical shift changes while the ^{13}C shifts of the methyl groups were relatively unperturbed or less significant over the larger ^{13}C chemical shift range. We therefore used this behavior to allow assignment of the methyl groups in the bound form without recourse to a full assignment. A sensitive HCCH-TOCSY spectrum of the bound form could be acquired to allow the ^{13}C shifts of the methyl groups for Leu, Val, and Ile to be assigned. Although the ^{13}C methyl region of the HCCH-TOCSY spectrum generally has several methyl groups on any one slice of the spectrum (digital resolution of 0.6 ppm), the *two* ^{13}C shifts of the methyls of Leu, Val, and Ile are generally unique to each residue. By utilizing two known ^{13}C shifts for each of the residues in the free form, a search close to both ^{13}C shifts in the HCCH-TOCSY spectrum reveals a set of symmetrically related peaks that identifies

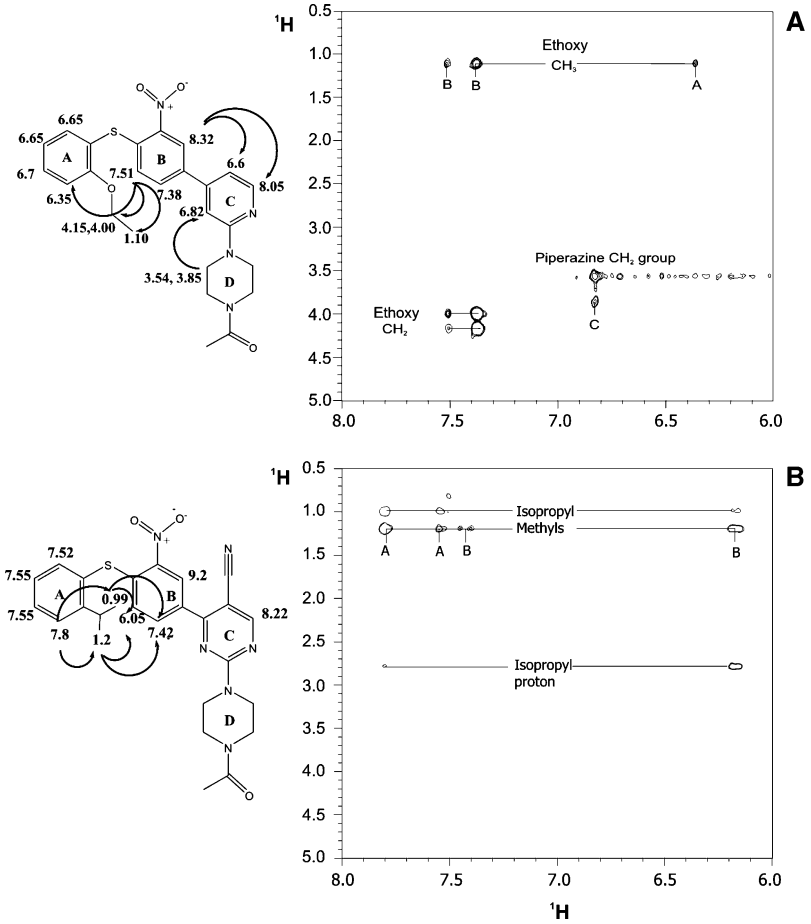

FIGURE 5: ^{15}N- and ^{13}C-filtered NOESY spectra of **1** and **2** bound to (125−311,C125A,W189R). Spectrum 1 (A) shows an expansion of the 2D ^{15}N- and ^{13}C-filtered NOESY fingerprint region of **1** in the bound form. The chemical shifts of protons on each ring are indicated with the corresponding ring letter, and the assignments of the intraring NOEs are given. A summary of the intraring NOEs is shown against the molecular structure of **1** with arrows indicating the proton pairs for which NOEs were determined. Spectrum 2 (B) shows an identical analysis for compound **2**.

the two methyl groups. To test this approach, complete backbone and side chain assignments were first made for (125−311,C125A,W189R). The assignments agreed well with published shifts with the exception of the mutated sites and several residues in contact with them (*29*). Within the seven groupings of residues that were shifted in the ^{15}N−^{1}H TROSY-HSQC spectrum, we identified a subset of hydrophobic residues that projected inward within the cavity and were most likely to interact with **1**. These included Val130, Leu132, Val157, Leu161, Val233, Ile235, Ile237, Ile255, Ile259, Ile261, Leu289, Leu298, and Leu302. Compound **1** was titrated into the solution of the I-domain to form a 1:1 complex and an HCCH-TOCSY spectrum recorded under identical conditions as previously for the free I-domain. For each of the 13 residues, the ^{1}H and ^{13}C shifts of their side chain methyl groups were compared with the chemical shifts in the free I-domain. Figure 4 shows a comparison of Leu132 methyl chemical shifts in the free and bound forms. As predicted, large ^{1}H chemical shift changes have been induced but the two methyl groups give an identifiable symmetric set of peaks on the same or adjacent planes of the HCCH-TOCSY spectrum of the free form. We found that at most it was necessary to search at least two planes (±1.2 ppm) in the HCCH-TOCSY spectrum of the bound form. The transfer of magnetization down to the Cα proton gave a second chemical shift that was surprisingly invariant between the free and bound form and provided a check on the assignment that was made. Chemical shift perturbations in the bound form were observed and assigned for the 13 residues identified as binding probes. It was estimated to take only 1−2 h to obtain the necessary assignments.

The next step was to search for NOEs from the aromatic ring system of **1** to these groups by using filtering and editing experiments. To achieve this, we utilized 2D filtering experiments as these were rapid to acquire and simple to interpret. First, application of ^{13}C and ^{15}N double-filtered TOCSY and NOESY experiments allowed the assignment of the protons of **1** in the bound form and the identification of the inhibitor intramolecular NOEs (see the Supporting Information). Assignment of NOEs in the I-domain−**1** complex was then easily achieved by the application of isotope filtering and editing experiments (Figure 5A). For **1**, 10 inhibitor intramolecular NOEs were identified through the use of ^{13}C and ^{15}N double-filtered TOCSY (for assignment) and NOESY experiments. These defined the dihedral angles between ring A and ring B and indicated that the ethoxy group of ring A was interacting with the *meta* and *ortho* protons of ring B. Second, interactions between the *ortho* proton of ring B and protons *para* and *meta* to the piperazine group defined the orientation of rings B and C.

We extended this analysis to the complex of (125−311,C125A,W189R) with **2**. Titration of **2** into solutions of the ^{15}N-labeled (125−311,C125A,W189R) gave similar chemical shift changes in the ^{15}N−^{1}H TROSY-HSQC spectra

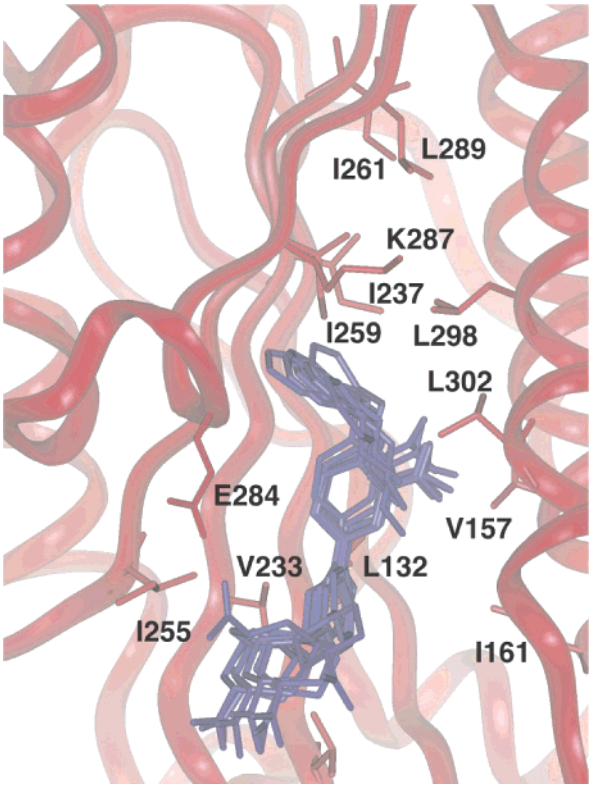

FIGURE 6: Ribbon representation of the backbone of (125−311,C125A,W189R) (red) with the superimposed coordinates of bound **1** overlaid (blue). The side chains of selected hydrophobic residues of the I-domain (leucines, isoleucines, and valines) that show methyl shifts in the bound form of **1** are also shown.

and was indicative once more of tight binding. Using a ^{13}C- and ^{15}N-labeled sample of (125−311,C125A,W189R) in complex with **2**, we carried out a second set of ^{13}C and ^{15}N double-filtered TOCSY and NOESY experiments (Figure 5B). Once again, we observe an excellent signal-to-noise ratio and well-resolved spectra that enabled us to discern that the dihedral angle between rings A and B is similar to that observed with compound **1**.

The final stage was to identify a number of intermolecular inhibitor−protein NOEs to orient **1** within the pocket. For this, we carried out a 2D ^{15}N-filtered NOESY experiment and identified NOEs between the shifted methyl peaks we observed in the HCCH-TOCSY experiment and the aromatic ring protons of **1** identified in the ^{13}C and ^{15}N double-filtered TOCSY experiments. Nine NOEs were rapidly identified arising from rings B and C. Ring B interacts with Leu132, Leu161, Val233, and Ile235, while ring C interacts with Leu132, Leu161, and Val233. Ten models were calculated using the X-ray coordinates of LFA-1 (with no bound ligand) and the ligand manually docked near the IDAS (20 Å from the diaryl bridge to the approximate center of the IDAS). A dynamic simulated annealing protocol was then applied where the majority of the residues in the I-domain were kept fixed during the calculations except those within 5 Å of inhibitor **1**. A superposition of 10 models for **1** bound to the X-ray structure of LFA-1 is shown in Figure 6. The combination of 10 intramolecular NOEs and 9 intermolecular NOEs yields a model where rings A−C are surprisingly well defined. NOEs between rings A and B orient the ethoxy group on ring A away from the binding pocket. This orientation of the rings was unexpected but was immediately apparent from our analysis of the ^{13}C- and ^{15}N-filtered NOESY data. This orientation differs from that observed in the NMR structures of other related diaryl I-domain inhibitors where the side chain of ring A points into the cavity. The analysis did not reveal any protein−inhibitor NOEs for ring D, and in the 10 structures that were generated, the group projects away from the binding pocket. Ring D shows broad signals in both the free and bound form, most likely due to conformational exchange in the ring backbone. The broader signals will tend to reduce the intensity of observed NOE signals and could prevent observation of any NOE buildup between the ring and the protein. Alternatively, ring C is rather better defined, and its positioning necessitates that ring D project away from the binding pocket; the lack of NOEs is most likely real.

In combination with ^{15}N-filtered NOESY experiments, we identified three inter-ring NOEs and 15 protein−inhibitor NOEs for compound **2**. Although we did not explicitly calculate a three-dimensional structure of the complex, the distribution of the NOEs over rings A−C in **2** indicated that this would be achievable and give models similar in quality to those with compound **1**. The observed NOEs indicate a bound conformation comparable to compound **1** with similar NOEs seen from each of the rings.

X-ray Crystallography and Comparison with the NMR-Derived Structure. An X-ray analysis was completed on the inhibitor−LFA-1 complex to determine if both X-ray and NMR gave comparable inhibitor-bound conformations. The purified I-domain expressed in *Escherichia coli* was complexed with the inhibitor and crystallized in space group *P*1 with four molecules in the asymmetric unit. Crystals were mounted in a cryostream, and diffraction patterns to 2.4 Å were collected. The data collection and refinement statistics for the inhibitor complex are given in Table 1.

The difference map revealed that the compound had bound in the IDAS in an orientation similar to that observed previously for this class of diaryl sulfides (*34*). The 2σ difference map is shown in Figure 7. The difference map was calculated using phases from the protein model, using differences in *F* values from the complex minus calculated *F* values from the protein model. No information about the compound was used for this calculation, to give an unbiased view of the compound electron density. Related compounds in the series bind in the same manner (data not shown and ref *34*).

A contact analysis was performed, and the residues that lie within 4 Å of the molecule include L132, F134, F153, V157, Y166, V233, I235, I255, Y257, I258, I259, E284, F285, V286, K287, L298, E301, L302, and K305. These are also illustrated in Figure 7. These residues are a subset of those that are identified as being perturbed in the NMR binding study but include nine of the aliphatic residues whose methyl groups were shifted upon binding of **1**. Those that are farther away may shift due to secondary effects upon binding.

Figure 8 shows an overlay of the average NMR- and X-ray-derived structures of the **1**−I-domain complex which superimpose with an rmsd of 1.53 Å. In blue and green are the average NMR structure and X-ray structure of bound inhibitor **1**, respectively. The overlay shows the similarity in the curvature of **1**, with rings A and D bending away from the linear arrangement of rings B and C. The translational

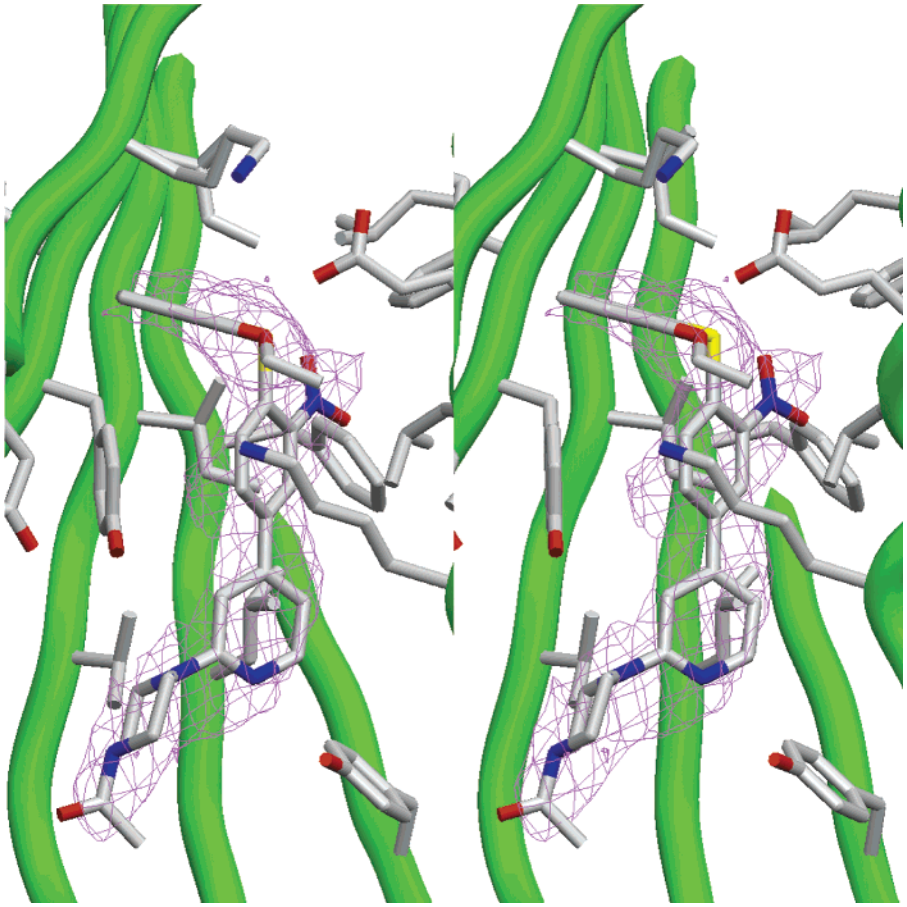

FIGURE 7: Stereoview of the difference map ($F_{obs-complex} - F_{calc-proteinmodel}$) contoured at 2σ showing the unbiased electron density of the bound inhibitor. The phases used for calculation came from the protein only. The compound was not included in the model for difference map calculation, and the observed electron density is due to the compound which is bound at this site. The position of the compound that is shown is in its final refined position, after it has been added to each of the four molecules in the asymmetric unit. The residues within 4 Å of the inhibitor are shown.

positioning of the inhibitor agrees closely with the X-ray structure, with only small differences seen for rings B and C along the *Y*-axis. The two structures agree along the *X*- and *Z*-axes. However, there is greater variation of the orientation of all four rings. For ring A, the ethoxy group points away from the cleft in both structures, showing contacts as expected to the protons *meta* and *para* to the nitro group of ring B. However, in the NMR structure, the angle between rings A and B brings the ethoxy group further over the plane of ring B and closer to the nitro substituent. Ring A is only constrained in the NMR calculations by contacts with ring B, and a lower precision for this ring might be expected. For ring B, the nitro group faces into the cleft in both structures and there is a 30° difference in the tilt of the ring. Ring B has more NOEs defining it and accordingly shows the best match with the X-ray structure. For ring C, the same side of the ring faces into cleft in each of the structures but there is a nearly 90° rotation of the ring C out of the plane observed in the X-ray structure. There is little structural information included for ring D in the NMR calculations, and in the X-ray structure, the electron density is poorly defined for this end of the inhibitor. However, in both structures, ring D is projected away from the binding pocket, providing the desired anchor point for solubilizing groups.

We collected X-ray data for the complex with compound **2** (data not shown) that confirmed a similar mode of binding to **1**, with ring D projected away from the pocket and a similar dihedral angle between rings A and B. However, the cyano substitution on ring C may have reduced the binding affinity of this adduct which had a measured IC_{50} of 404 nM, versus a value of 10.9 nM for **1**.

Application to Structure-Aided Drug Design. A combination of ITC, NMR, and X-ray techniques has been used to characterize the binding of a four-ring inhibitor of the IDAS of the LFA-1 I-domain. Commonly, ITC experiments involve titrating the small molecule into a solution of the macromolecule of interest. This method requires an inhibitor concentration in excess of 100 μM, making it unsuitable for sparingly soluble molecules such as **1**. This practical problem is overcome by reversing the reagent addition so that reliable data can be obtained from inhibitor solution concentrations in the range of 5−20 μM. In this way, we were able to show that the inhibitor binds to the LFA-1 I-domain with a K_d of 18.3 nM. Since in the DELFIA format, binding of ICAM to LFA-1 occurs on a surface, it is not ideal for determining true dissociation constants for competing molecules. Nonetheless, the K_d value generated by ITC is close enough to the IC_{50} (10.9 nM) to suggest that the affinity of **1** for LFA-1 is purely a function of I-domain binding.

Comparison of the two structures using a minimal set of NMR distance restraints reveals the essential topological features of the bound inhibitor and positioning within the IDAS of the I-domain. The design of inhibitors of LFA-1

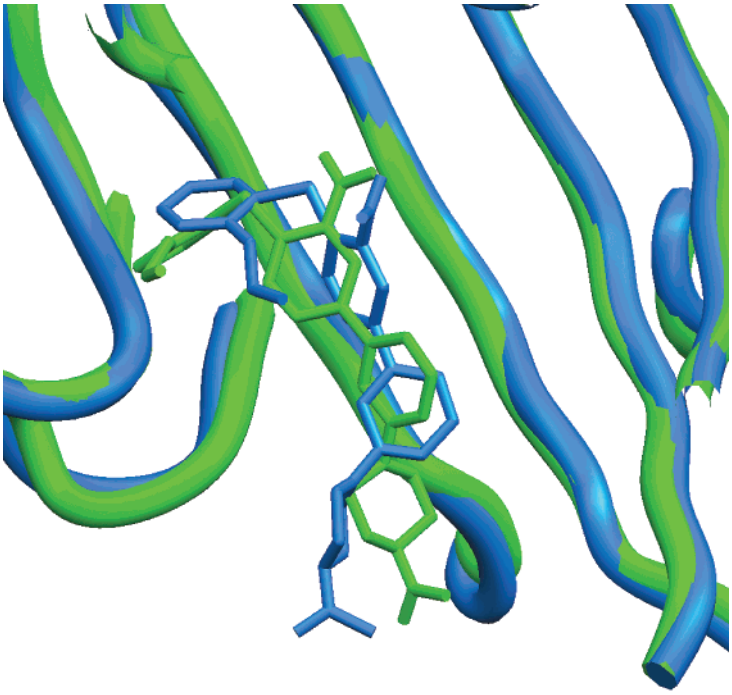

FIGURE 8: Comparison of the average NMR model of **1**-bound (125−311,C125A,W189R) with the X-ray-derived structure. The X-ray structure is shown in green, and the NMR structure is shown in blue.

has reached a point where subtle changes are being made to slowly increment the binding affinity of the inhibitors. While crystallization studies of some of these lead compounds are attempted, it is not generally considered feasible for all such complexes to be fully structurally characterized. On the other hand, a fast and simple NMR titration produces only a rough map of the binding site, but when the three-dimensional inhibitor structure is being refined, this clearly does not give sufficiently accurate information about the bound conformation. We have chosen an intermediate analysis where we seek to gain a total of 10−20 inhibitor intramolecular and inhibitor protein intermolecular restraints from a subset of readily observable methyl groups in the binding pocket. This information can be acquired with a single HCCH-TOCSY experiment and 2D ^{15}N-filtered and ^{15}N- and ^{13}C-filtered TOCSY and NOESY experiments and could be applicable to other complexes of this size and larger with modifications to the TOCSY experiment. Previously, the use of isotope-filtered 2D HOHAHA spectroscopy with a peptide−protein complex using heteronuclear Hartmann−Hahn dephasing has been reported (*44*). A pulse sequence was used that avoided the additional purging delays during which rapid transverse relaxation can significantly attenuate signals in larger complexes. This gave nearly complete assignments for a pepetide in a 20 kDa complex and was also reported to be effective in studying significantly larger complexes.

Analysis of the spectra is fast, and the results give structures that reveal the *same* important features in both the NMR and X-ray structures. These properties can be provided to synthetic teams to help lead the design of the next generation of inhibitors. Extension to a related molecule in this inhibitor class (**2**) provides essential information, such as how the substitution of the ethoxy group on ring A (**1**) for the isopropyl group (**2**) retains the unusual dihedral angle between rings A and B (Figure 5). In addition the introduction of the preordering, ring C has had the desired effect and projects ring D away from the binding pocket, making it ready to provide an anchor point for solubilizing groups (*36*). The method does not intend to compete with X-ray crystallography in terms of accuracy, and the results would not be, for example, suitable as the basis for a molecular modeling analysis of the bound conformation.

A recognition of the importance of this integrin has led to an increased intensity of research in this area in recent years. This has continued to generate new classes of inhibitors such as the 1,4-diazepane-2-ones (*33*) and *N*-benzoyl amino acids (*45*) and their derivatives. These classes as well as the diaryl sulfides require extensive derivatization for optimization of their pharmacokinetic profiles, and rapid structural screening can aid significantly in this process. We have applied this approach to the optimization of two diaryl sulfides and shown NMR can rapidly provide a structural model of the inhibitor in the bound form as an alternative to X-ray crystallography. The alternative more accurate assay for the determination of the inhibitor K_d will aid in better characterization of further inhibitors.

ACKNOWLEDGMENT

We thank Gunter Stier for providing a TEV protease-producing *E. coli* strain, Daruka M. for the initial cloning of the I-domain, Lloyd King for the mass spectroscopy measurements, and Jeff Kenedy for performing the DELFIA assays.

SUPPORTING INFORMATION AVAILABLE

^{1}H chemical shifts of **1** in the free and bound forms. This material is available free of charge via the Internet at http://pubs.acs.org.

REFERENCES

1. Shimaoka, M., Takagi, J., and Springer, T. A. (2002) Conformational regulation of integrin structure and function, *Annu. Rev. Biophys. Biomol. Struct. 31*, 485−516.
2. Harris, E. S., McIntyre, T. M., Prescott, S. M., and Zimmerman, G. A. (2000) The leukocyte integrins, *J. Biol. Chem. 275*, 23409−23412.
3. Stewart, M., Thiel, M., and Hogg, N. (1995) Leukocyte integrins, *Curr. Opin. Cell Biol. 7*, 690−696.
4. Winquist, R. J., Desai, S., Fogal, S., Haynes, N. A., Nabozny, G. H., Reilly, P. L., Souza, D., and Panzenbeck, M. (2001) The role of leukocyte function-associated antigen-1 in animal models of inflammation, *Eur. J. Pharmacol. 429*, 297−302.
5. Berlin-Rufenach, C., Otto, F., Mathies, M., Westermann, J., Owen, M. J., Hamann, A., and Hogg, N. (1999) Lymphocyte migration in lymphocyte function-associated antigen (LFA)-1-deficient mice, *J. Exp. Med. 189*, 1467−1478.
6. Papp, K., Bissonnette, R., Krueger, J. G., Carey, W., Gratton, D., Gulliver, W. P., Lui, H., Lynde, C. W., Magee, A., Minier, D., Ouellet, J. P., Patel, P., Shapiro, J., Shear, N. H., Kramer, S., Walicke, P., Bauer, R., Dedrick, R. L., Kim, S. S., White, M., and Garovoy, M. R. (2001) The treatment of moderate to severe psoriasis with a new anti-CD11a monoclonal antibody, *J. Am. Acad. Dermatol. 45*, 665−674.
7. Xiong, J.-P., Stehle, T., Diefenbach, B., Zhang, R., Dunker, R., Scott, D. L., Joachimiak, A., Goodman, S. L., and Arnaout, M. A. (2001) Crystal structure of the extracellular segment of integrin αvβ3, *Science 294*, 339−345.
8. Xiong, J.-P., Stehle, T., Zhang, R., Joachimiak, A., Frech, M., Goodman, S. L., and Arnaout, M. A. (2002) Crystal structure of the extracellular segment of integrin αvβ3 in complex with an Arg-Gly-Asp ligand, *Science 296*, 151−155.
9. Huang, C., and Springer, T. A. (1995) A binding interface on the I domain of lymphocyte function-associated antigen-1 (LFA-1) required for specific interaction with intercellular adhesion molecule 1 (ICAM-1), *J. Biol. Chem. 270*, 19008−19016.
10. Kamata, T., Wright, R., and Takada, Y. (1995) Critical threonine and aspartic acid residues within the I domains of β2 integrins for interactions with intercellular adhesion molecule 1 (ICAM-1) and C3bi, *J. Biol. Chem. 270*, 12531−12535.
11. Randi, A. M., and Hogg, N. (1994) I domain of β2 integrin lymphocyte function-associated antigen-1 contains a binding site for ligand intercellular adhesion molecule-1, *J. Biol. Chem. 269*, 12395−12398.
12. Leitinger, B., and Hogg, N. (2000) Effects of I domain deletion on the function of the β2 integrin lymphocyte function-associated antigen-1, *Mol. Biol. Cell 11*, 677−690.
13. Yalamanchili, P., Lu, C., Oxvig, C., and Springer, T. A. (2000) Folding and function of I domain-deleted Mac-1 and lymphocyte function-associated antigen-1, *J. Biol. Chem. 275*, 21877−21882.
14. Lee, J. O., Rieu, P., Arnaout, M. A., and Liddington, R. (1995) Crystal structure of the A domain from the alpha subunit of integrin CR3 (CD11b/CD18), *Cell 80*, 631−638.
15. Staunton, D. E., Dustin, M. L., Erickson, H. P., and Springer, T. A. (1990) The arrangement of the immunoglobulin-like domains of ICAM-1 and the binding sites for LFA-1 and rhinovirus, *Cell 61*, 243−254.
16. Emsley, J., Knight, C. G., Farndale, R. W., Barnes, M. J., and Liddington, R. C. (2000) Structural basis of collagen recognition by integrin α2β1, *Cell 101*, 47−56.
17. Bella, J., Kolatkar, P. R., Marlor, C. W., Greve, J. M., and Rossmann, M. G. (1998) The structure of the two amino-terminal domains of human ICAM-1 suggests how it functions as a rhinovirus receptor and as an LFA-1 integrin ligand, *Proc. Natl. Acad. Sci. U.S.A. 95*, 4140−4145.
18. Stanley, P., and Hogg, N. (2003) The I domain of integrin LFA-1 interacts with ICAM-1 domain 1 at residue Glu-34 but not Gln-73, *J. Biol. Chem. 273*, 3358−3362.
19. Shimaoka, M., Xiao, T., Liu, J. H., Yang, Y., Dong, Y., Jun, C. D., McCormack, A., Zhang, R., Joachimiak, A., Takagi, J., Wang, J. H., and Springer, T. A. (2003) Structures of the alpha L I domain and its complex with ICAM-1 reveal a shape-shifting pathway for integrin regulation, *Cell 112*, 99−111.
20. Qu, A., and Leahy, D. J. (1995) Crystal structure of the I-domain from the CD11a/CD18 (LFA-1, αLβ2) integrin, *Proc. Natl. Acad. Sci. U.S.A. 92*, 10277−10281.
21. Lee, J. O., Bankston, L. A., Arnaout, M. A., and Liddington, R. C. (1995) Two conformations of the integrin A-domain (I-domain): a pathway for activation? *Structure 3*, 1333−1340.
22. Shimaoka, M., Shifman, J. M., Jing, H., Takagi, J., Mayo, S. L., and Springer, T. A. (2000) Computational design of an integrin I domain stabilized in the open high affinity conformation, *Nat. Struct. Biol. 7*, 674−678.
23. Shimaoka, M., Lu, C., Palframan, R. T., von Andrian, U. H., McCormack, A., Takagi, J., and Springer, T. A. (2001) Reversibly locking a protein fold in an active conformation with a disulfide bond: integrin αL I domains with high affinity and antagonist activity in vivo, *Proc. Natl. Acad. Sci. U.S.A. 98*, 6009−6014.
24. Lu, C., Shimaoka, M., Zang, Q., Takagi, J., and Springer, T. A. (2001) Locking in alternate conformations of the integrin αLβ2 I domain with disulfide bonds reveals functional relationships among integrin domains, *Proc. Natl. Acad. Sci. U.S.A. 98*, 2393−2398.
25. Lu, C., Shimaoka, M., Ferzly, M., Oxvig, C., Takagi, J., and Springer, T. A. (2001) An isolated, surface-expressed I domain of the integrin αLβ2 is sufficient for strong adhesive function when locked in the open conformation with a disulfide bond, *Proc. Natl. Acad. Sci. U.S.A. 98*, 2387−2392.
26. Shimaoka, M., Lu, C., Salas, A., Xiao, T., Takagi, J., and Springer, T. A. (2002) Stabilizing the integrin αM inserted domain in alternative conformations with a range of engineered disulfide bonds, *Proc. Natl. Acad. Sci. U.S.A. 99*, 16737−16741.
27. Xiong, J.-P., Li, R., Essafi, M., Stehle, T., and Arnaout, M. A. (2000) An isoleucine-based allosteric switch controls affinity and shape shifting in integrin CD11b A-domain, *J. Biol. Chem. 275*, 38762−38767.
28. Kallen, J., Welzenbach, K., Ramage, P., Geyl, D., Kriwacki, R., Legge, G., Cottens, S., Weitz-Schmidt, G., and Hommel, U. (1999) Structural basis for LFA-1 inhibition upon lovastatin binding to the CD11a I-domain, *J. Mol. Biol. 292*, 1−9.
29. Legge, G. B., Kriwacki, R. W., Chung, J., Hommel, U., Ramage, P., Case, D. A., Dyson, H. J., and Wright, P. E. (2000) NMR solution structure of the inserted domain of human leukocyte function associated antigen-1, *J. Mol. Biol. 295*, 1251−1264.
30. Huth, J. R., Olejniczak, E. T., Mendoza, R., Liang, H., Harris, E. A., Lupher, M. L., Jr., Wilson, A. E., Fesik, S. W., and Staunton, D. E. (2000) NMR and mutagenesis evidence for an I domain allosteric site that regulates lymphocyte function-associated antigen 1 ligand binding, *Proc. Natl. Acad. Sci. U.S.A. 97*, 5231−5236.
31. Last-Barney, K., Davidson, W., Cardozo, M., Frye, L. L., Grygon, C. A., Hopkins, J. L., Jeanfavre, D. D., Pav, S., Qian, C., Stevenson, J. M., Tong, L., Zindell, R., and Kelly, T. A. (2001) Binding site elucidation of hydantoin-based antagonists of LFA-1 using multidisciplinary technologies: evidence for the allosteric inhibition of a protein−protein interaction, *J. Am. Chem. Soc. 123*, 5643−5650.
32. Liu, G., Link, J. T., Pei, Z., Reilly, E. B., Leitza, S., Nguyen, B., Marsh, K. C., Okasinski, G. F., von Geldern, T. W., Ormes, M., Fowler, K., and Gallatin, M. (2000) Discovery of novel *p*-arylthio cinnamides as antagonists of leukocyte function-associated antigen-1/intracellular adhesion molecule-1 interaction. 1. Identification of an additional binding pocket based on an anilino diaryl sulfide lead, *J. Med. Chem. 43*, 4025−4040.
33. Wattanasin, S., Albert, R., Ehrhardt, C., Roche, D., Sabio, M., Hommel, U., Welzenbach, K., and Weitz-Schmidt, G. (2003) 1,4-Diazepane-2-ones as novel inhibitors of LFA-1, *Bioorg. Med. Chem. Lett. 13*, 499−502.
34. Liu, G., Huth, J. R., Olejniczak, E. T., Mendoza, R., DeVries, P., Leitza, S., Reilly, E. B., Okasinski, G. F., Fesik, S. W., and von Geldern, T. W. (2001) Novel *p*-arylthio cinnamides as antagonists of leukocyte function-associated antigen-1/intracellular adhesion molecule-1 interaction. 2. Mechanism of inhibition and structure-based improvement of pharmaceutical properties, *J. Med. Chem. 44*, 1202−1210.
35. Shuker, S. B., Hajduk, P. J., Meadows, R. P., and Fesik, S. W. (1996) Discovering high-affinity ligands for proteins: SAR by NMR, *Science 274*, 1531−1534.
36. Pei, Z., Xin, Z., Liu, G., Li, Y., Reilly, E. B., Lubbers, N. L., Huth, J. R., Link, J. T., von Geldern, T. W., Cox, B. F., Leitza, S., Gao, Y., Marsh, K. C., DeVries, P., and Okasinski, G. F. (2001) Discovery of potent antagonists of leukocyte function-associated antigen-1/intercellular adhesion molecule-1 interaction. 3. Amide (C-ring) structure−activity relationship and improvement of overall properties of arylthio cinnamides, *J. Med. Chem. 44*, 2913−2920.

37. Bohmann, D., and Tjian, R. (1989) Biochemical analysis of transcriptional activation by Jun: differential activity of c- and v-Jun, *Cell 59*, 709−717.
38. Pervushin, K., Riek, R., Wider, G., and Wuthrich, K. (1997) Attenuated T_2 relaxation by mutual cancellation of dipole−dipole coupling and chemical shift anisotropy indicates an avenue to NMR structures of very large biological macromolecules in solution, *Proc. Natl. Acad. Sci. U.S.A. 94*, 12366−12371.
39. Brünger, A. T. (1993) *X-PLOR manual*, version 3.1, Yale University, New Haven, CT.
40. Kleywegt, G. J. (1995) XPLO-2D. Dictionaries for Heteros, *CCP4/ESF-EACBM Newsletter on Protein Crystallography 31*, 45−50.
41. Otwinowski, Z. (1993) *DENZO*, Yale University, New Haven, CT.
42. Collaborative Computational Project, Number 4 (1994) The CCP4 Suite: Programs for Protein Crystallography, *Acta Crystallogr. D50*, 760−763.
43. Jones, T. A., Zou, J.-Y., Cowan, S. W., and Kjeldgaard, M. (1991) Improved methods for binding protein models in electron density maps and the location of errors in these models, *Acta Crystallogr. A47*, 110−119.
44. Bax, A., Grzesiek, S., Gronenborn, A. M., and Clore, M. (1994) Isotope-Filtered 2D HOHAHA spectroscopy of a peptide−protein complex using heteronuclear Hartmann−Hahn dephasing, *J. Magn. Reson., Ser. A 106*, 269−273.
45. Burdick, D. J., Paris, K., Weese, K., Stanley, M., Beresini, M., Clark, K., McDowell, R. S., Marsters, J. C., and Gadek, T. R. (2003) N-Benzoyl amino acids as LFA-1/ICAM inhibitors 1: amino acid structure−activity relationship, *Bioorg. Med. Chem. Lett. 13*, 1015−1018.

BI035422A